SEECCM III
3rd South-East European Conference on Computational Mechanics-
an ECCOMAS and IACM Special Interest Conference
M. Papadrakakis, M. Kojic, I. Tuncer (eds.)
Kos Island, Greece, 12–14 June 2013

VIBRATION AND ELASTIC BUCKLING ANALYSES OF SINGLE-WALLED CARBON NANOCONES

Cengiz Baykasoglu[1], Alper T. Celebi[1], Esra Icer[1] and Ata Mugan[1]

[1]: Istanbul Technical University, Faculty of Mechanical Engineering, 34437, Istanbul, Turkey

e-mails: baykasoglu@itu.edu.tr, *celebial@itu.edu.tr, icere@itu.edu.tr, mugan@itu.edu.tr

Keywords: Single-Walled Carbon Nanocones, Vibration Analysis, Buckling Analysis, Molecular Mechanics, Finite Element Method.

Abstract. *This paper reports the result on elastic buckling and vibration behaviors of single-walled carbon nanocones (SWCNCs) having the potential usage in atomic force microscope and scanning tunneling microscope tips. The modeling work employs the molecular mechanics based finite element approach in which Euler-Bernoulli beam element formulations are used with consistent mass matrix. Free-free, free-clamped and clamped-clamped boundary conditions are considered in vibration analysis of SWCNCs; on the other hand, axial compression and bending loading conditions are taken into account in elastic buckling behavior of SWCNCs. The effects of cone height and disclination or apex angles on the buckling force and natural frequencies of SWCNCs are investigated. Vibration analysis results indicate that the natural frequency decreases with increasing cone height in all types of SWCNCs, whereas it increases as the disclination angle increases. Buckling analysis results indicate that as the disclination angle increases, the critical buckling load increases in axial compression loading and decreases in bending loading. In addition, it is observed that bending loading is more critical than axial compression loading for buckling behavior of SWCNCs if the disclination angle increases.*

1 INTRODUCTION

Since the experimental detection of carbon nanotubes (CNTs) in 1991 [1], extensive studies have been conducted on its extraordinary properties and researchers have been interested in other carbon based nanostructures such as graphene sheets (GSs), fullerenes and carbon nanocones (CNCs). CNCs are conical graphitic structures and have very promising mechanical, electrical and thermal properties [2-7]. Ge and Sattler [8] first proposed that five apex angles such as 19.2°, 38.9°, 60°, 86.6° and 123.6° can be used to distinguish CNCs . Krishnan et al. [9] verified the existence of the five types of CNCs experimentally. CNCs are suited for high resolution and/or high intensity applications due to its small size, high stiffness and conical geometry; thus, it can be used as scanning probe tips (i.e., atomic force microscope (AFM) and scanning tunneling microscope (STM) probes), electron field emitters and in nanoindentation applications [9-13].

Understanding the mechanical behavior of CNCs is important and very useful in designing the components having nanocone structures. Experimental measurements for prediction of the mechanical properties of CNCs are very difficult and costly. Thus, computational tools are widely used to characterize mechanical properties of CNCs [6, 7, 14-17, 28]. Kumar et al. [6] investigated the Young's and shear modulus of CNCs employing second-generation reactive empirical bond-order potential. Wei et al. [7] examined the elastic and plastic properties of SWCNCs by using molecular dynamics (MD) simulations. Tsai and Fang [14] and Liew et al. [15] analyzed the buckling behavior of CNCs by using MD simulations. Liao et al. [16] investigated tensile and compressive behaviors of open-tip CNCs employing MD simulations. Abadi et al. [17] studied free vibrational properties of CNCs based on a nonlocal continuum shell model. Atomistic based finite element (FE) modeling approaches have been used to analyze CNCs and other carbon based structures in many recent works in literature due to its computational time and cost advantages. Odegard et al. [18] developed a model that links the molecular mechanics and solid mechanics, which is established by equating the molecular potential energy terms with the mechanical strain energy of a representative volume element of a continuum model. Li and Chou in the works [19-22] developed a similar approach to model CNTs and GSs similar to space-frame structures and investigated the elastic, vibrational and buckling characteristics of CNTs and/or GSs. Cantilevered and bridged single walled carbon nanotubes (SWCNTs) are taken into account to predict fundamental frequencies of SWCNTs [21] that are found to be in the range of 10 GHz –1.5 THz. Both axial compression and bending loading conditions are considered in the elastic buckling behavior of the CNTs in [22] where buckling forces are reported to be in the range of ~0.1– 39 nN. Li and Chou [22] reported that the buckling load in axial compression is higher than bending load. Tserpes and Papanikos [23] introduced an atomistic FE method based on the approach of Li and Chou [19] to model CNTs by using commercial FE codes; they identified the C-C bond thickness d, Young's modulus E and shear modulus G by using the AMBER force model [19]. By using the methods developed by Li and Chou [19] and Tserpes and Papanikos [23]; Hashemnia et al. [24] and Sakhaee-Pour et al. [25] examined natural frequencies and mode shapes of single-layered graphene sheets (SLGSs) and Sakhaee-Pour et al. [25] predicted fundamental frequencies of SLGSs with equivalent lengths that are found to be in the range of 2.4 GHz – 3.5 THz; Sakhaee-Pour et al. [26] studied natural frequencies and mode shapes SWCNTs; Sakhaee-Pour [27] analyzed elastic buckling of SLGSs; Lee and Lee [28] studied vibrational behaviors of SWCNTs and SWCNCs, and predicted fundamental frequencies of SWCNCs below 20 GHz with a cone having the height of 20 Å; Mir et al. [29] studied natural frequencies and mode shapes of SWCNTs; Cheng et al. [30] and Fan et al. [31] examined mechanical properties of CNTs such as Young's modulus, shear modulus, natural frequency and buckling load;

Avila et al. [32] analyzed elastic and vibrational properties of GSs and CNTs; we studied two- and three-dimensional modal and transient analyses of SLGSs in [33]. In the works [19 -27, 29, 30-33], Euler-Bernoulli beam elements are used to represent bond interactions between C-C atoms in GSs, CNTs and CNCs. In addition, in the works [20, 21, 24-26, 28, 31,32] studying the vibrations of GSs, CNTs and CNCs, the global mass matrix is derived based on the assumption that the carbon nuclei masses are concentrated at the joints of the frame structure in GSs, CNTs and CNCs, and lumped mass matrix for the beam elements is used. On the other hand, consistent mass matrices for Euler-Bernoulli beam elements are used in the studies [29, 33]. In Mir et al. [29], density of beam elements is selected to be the density of continuum model of GSs (i.e., 2300 kg/m3) in the MM models (i.e., see Table 1). However, due to this assumption, the total mass of the MM model is different from the mass of the original structure which also affects the associated natural frequencies. In the work [33], equivalent density parameter for the beam elements is derived by using the equivalency of natural frequencies of the MM model and continuum plane-stress FE model of SLGSs that is found to be 5500 kg/m3. It is noteworthy that transient dynamics analyses can be performed by using Newmark method due to the advantages of consistent mass matrix which does not yield singularity in numerical integrations. On the other hand, Scarpa and Adhikari [34,35] proposed a beam model considering the shear deformation effects and they found the C-C bond thickness d , Poisson's ratio ν, Young's modulus E and shear modulus G by using the AMBER force model constants [19]. Both of the models in Li and Chou [19] and Scarpa and Adhikari [34] yield the same deformation results as the structural mechanics stiffness constants in the AMBER force model are equal [33] if the corresponding element properties are used given in Table 1. Lee and Lee [28] used Timoshenko beam element formulations which include shear deformation effects but they employed Euler-Bernoulli beam element constants (i.e., see Table 1) [23]; this assumption affects the natural frequencies of SWCNC that are found to be lower than those of Euler-Bernoulli beam elements. If shear deformation effects are considered, parameters of shear beam formulations given in Scarpa and Adhikari [34, 35] should be used.

Even though there are some studies on nanocones, no study exists on buckling behavior of SWCNCs by using atomic based FE approach. In addition, Lee and Lee [28] studied of vibrations of SWCNCs; however, they did not examine the effects of cone height and used Timoshenko beam formulations with Euler-Bernoulli beam parameters which may lead to lower modal frequencies than actual values. Motivated by these facts, vibration and elastic buckling analysis of SWCNCs are completed by using the MM based FE approach [19, 23] where Euler-Bernoulli beam elements with consistent mass matrix are used. In vibration analysis of SWCNCs, free-free, free-clamped and clamped-clamped boundary conditions are considered. Axial compression and bending loading conditions are taken into account in the elastic buckling behavior of the SWCNCs. In all analyses, the disclination angles of 120°, 180° and 240° are used while the cone height is varying.

2 FE MODEL OF SWCNCs

2.1 Structures of SWCNCs

The GSs are the basic structural elements of CNTs, CNCs and fullerenes, and their geometry is uniquely determined. However, a lot of possibility exists for CNTs (i.e., armchair, zigzag and chiral types CNTs) and CNCs having five possible closed cone structures that can be constructed by using GSs [36, 37]. By rotating a fragment of GSs in multiples of 60°, we obtain the original structure due to the hexagonal symmetry of GSs that is the only way to generate smoothly joined CNC by folding over a GS and the overlaps are called the disclinations.

Folding over a GS in this manner, creates five possible closed distinct CNC structures and the apex angles of a cone can be calculated as follows [38]

$$\alpha = 2\arcsin(1-\frac{\theta}{360}) \tag{1}$$

where θ is the disclination angle in degrees. Taking θ as 60°, 120°, 180°, 240° and 300°, the apex angles of CNCs are calculated 112.9°, 83.6°, 60°, 38,9° and 19.2°, respectively. The CNTs can be seen as a special case of the CNCs with a zero apex angle.

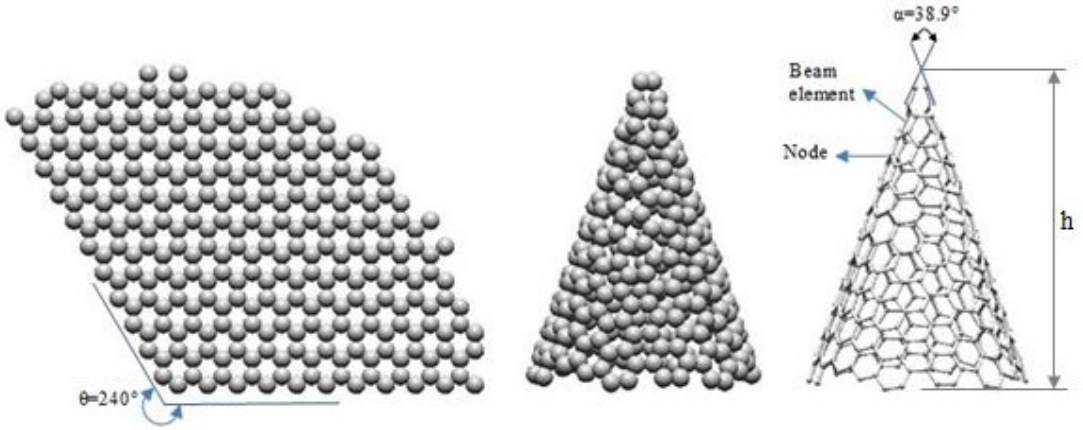

Figure 1: The cone sheet with the dislocation angle of 240° corresponding to the cone with apex angle of 38.9° SWCNC and its equivalent FE model.

Figure 1 shows the cone sheet with the dislocation angle of 240° corresponding to the cone with apex angle of 38.9° SWCNC and its equivalent FE model. Other types of SWCNCs and FE models can be produced in a similar way as shown in Figure 1. The larger the apex angle of a SWCNC, the larger the bottom radii and number of atoms.

2.2 Application of atomistic FE modeling approach to SWCNCs

For the simulation of vibration and elastic buckling behaviors of SWCNCs, an atomistic FE modeling approach is used. When carbon based nanostructures such as GSs, CNTs and CNCs are subjected to external forces, the positions of the atomic nuclei are controlled by the covalent bonds between C-C atoms. Hence, the deformation pattern of these nanostructures is very similar to deformation of the frame structures. To this end, SWCNCs are modeled as 3-D space frame-like structures in simulations and a covalent bond between two carbon atoms is represented by an Euler-Bernoulli beam element having consistent mass matrices (i.e., see Figure 1). The element stiffness matrix and consistent mass matrix for a 3-D Euler-Bernoulli beam element are given by Equations (2) and (3), respectively.

$$\boldsymbol{K} = \begin{bmatrix} K_{ii} & K_{ij} \\ K_{ij} & K_{jj} \end{bmatrix} \quad \boldsymbol{M} = \begin{bmatrix} M_{ii} & M_{ij} \\ M_{ij} & M_{jj} \end{bmatrix} \tag{2}$$

where the sub-matrices, K_{ii}, K_{ij}, K_{jj}, M_{ii}, M_{ij} and M_{jj} are given by

$$K_{ii}=\begin{bmatrix} \frac{EA}{L} & 0 & 0 & 0 & 0 & 0 \\ 0 & \frac{12EI_x}{L^3} & 0 & 0 & 0 & \frac{6EI_x}{L^2} \\ 0 & 0 & \frac{12EI_y}{L^3} & 0 & -\frac{6EI_y}{L^2} & 0 \\ 0 & 0 & 0 & \frac{GJ}{L} & 0 & 0 \\ 0 & 0 & -\frac{6EI_y}{L^2} & 0 & \frac{4EI_y}{L} & 0 \\ 0 & \frac{6EI_x}{L^2} & 0 & 0 & 0 & \frac{4EI_x}{L} \end{bmatrix}, \quad K_{ij}=\begin{bmatrix} -\frac{EA}{L} & 0 & 0 & 0 & 0 & 0 \\ 0 & -\frac{12EI_x}{L^3} & 0 & 0 & 0 & \frac{6EI_x}{L^2} \\ 0 & 0 & -\frac{12EI_y}{L^3} & 0 & -\frac{6EI_y}{L^2} & 0 \\ 0 & 0 & 0 & -\frac{GJ}{L} & 0 & 0 \\ 0 & 0 & -\frac{6EI_y}{L^2} & 0 & \frac{2EI_y}{L} & 0 \\ 0 & -\frac{6EI_x}{L^2} & 0 & 0 & 0 & \frac{2EI_x}{L} \end{bmatrix}$$

$$K_{jj}=\begin{bmatrix} \frac{EA}{L} & 0 & 0 & 0 & 0 & 0 \\ 0 & \frac{12EI_x}{L^3} & 0 & 0 & 0 & -\frac{6EI_x}{L^2} \\ 0 & 0 & \frac{12EI_y}{L^3} & 0 & \frac{6EI_y}{L^2} & 0 \\ 0 & 0 & 0 & \frac{GJ}{L} & 0 & 0 \\ 0 & 0 & \frac{6EI_y}{L^2} & 0 & \frac{4EI_y}{L} & 0 \\ 0 & -\frac{6EI_x}{L^2} & 0 & 0 & 0 & \frac{4EI_x}{L} \end{bmatrix}, \quad M_{ii}=\rho AL\begin{bmatrix} \frac{1}{3} & 0 & 0 & 0 & 0 & 0 \\ 0 & \frac{13}{35} & 0 & 0 & 0 & \frac{11L}{210} \\ 0 & 0 & \frac{13}{35} & 0 & -\frac{11L}{210} & 0 \\ 0 & 0 & 0 & \frac{J}{3A} & 0 & 0 \\ 0 & 0 & -\frac{11L}{210} & 0 & \frac{L^2}{105} & 0 \\ 0 & \frac{11L}{210} & 0 & 0 & 0 & \frac{L^2}{105} \end{bmatrix}$$

$$M_{ij}=\rho AL\begin{bmatrix} \frac{1}{6} & 0 & 0 & 0 & 0 & 0 \\ 0 & \frac{9}{70} & 0 & 0 & 0 & \frac{13L}{420} \\ 0 & 0 & \frac{9}{70} & 0 & -\frac{13L}{420} & 0 \\ 0 & 0 & 0 & \frac{J}{6A} & 0 & 0 \\ 0 & 0 & \frac{13L}{420} & 0 & -\frac{L^2}{140} & 0 \\ 0 & -\frac{13L}{420} & 0 & 0 & 0 & -\frac{L^2}{140} \end{bmatrix}, \quad M_{jj}=\rho AL\begin{bmatrix} \frac{1}{3} & 0 & 0 & 0 & 0 & 0 \\ 0 & \frac{13}{35} & 0 & 0 & 0 & -\frac{11L}{210} \\ 0 & 0 & \frac{13}{35} & 0 & \frac{11L}{210} & 0 \\ 0 & 0 & 0 & \frac{J}{3A} & 0 & 0 \\ 0 & 0 & \frac{11L}{210} & 0 & \frac{L^2}{105} & 0 \\ 0 & -\frac{11L}{210} & 0 & 0 & 0 & \frac{L^2}{105} \end{bmatrix} \tag{3}$$

where L denotes the initial length of a C-C bond and equals to 0.1421 nm. In addition, for the computational model, numerical values of the following stiffness parameters should be given a priori: A is the cross-sectional area, E and G are respectively the Young's and shear moduli, I and J are respectively the moment of inertia and polar moment of inertia of the cross section and ρ is the beam element density. To obtain E, G, A, I and J, energy equivalence concept is employed. In this analogy, stretching, bending and twisting potential energy terms based on the MM and structural mechanics models are assumed to be independent of each other and then corresponding terms are set equal to each other in these two models. Under the small deformation assumption and by using harmonic expressions of potential energy in the MM model, Li and Chou [19] obtained the following relations by using energy equivalence concept

$$\frac{EA}{L}=k_r,\ \frac{EI}{L}=k_\theta,\ \frac{GJ}{L}=k_\tau \tag{4}$$

where k_r, k_θ and k_τ respectively denote the bond stretching, angle bending and torsional force constants, respectively. Assuming that the cross section of beam elements is uniform and circular, then the Young's modulus E, the shear modulus G and diameter of the cross sec-

tion d are obtained by plugging in the cross sectional area $A=\pi d^2/4$, moment of inertia $I_x=I_y=\pi d^4/64$ and polar moment of inertia $J=\pi d^4/32$ as follows [23]

$$E=\frac{k_r{}^2 L}{4\pi k_\theta},\ G=\frac{k_r{}^2 k_\tau L}{8\pi k_\theta^2}\ \ d=4\sqrt{\frac{k_\theta}{k_r}} \tag{5}$$

In this study, the AMBER force model is chosen [19, 23]. The AMBER force model constants k_r , k_θ and k_τ are taken as $6.52\times10^{-7}Nnm^{-1}$, $8.76\times10^{-10}Nnmrad^{-2}$ and $2.78\times10^{-10}Nnmrad^{-2}$, respectively. Table (1) summarizes the properties of the Euler-Bernoulli beam element which are the inputs of the FE models.

2.3 Vibrational and buckling analyses of SWCNCs

In this study, SWCNCs with disclination angles of 120°, 180° and 240° are taken into account which satisfied the continuity condition at the folding of the cone sheet. The tip of the SWCNCs is not explicitly modeled in vibrational and buckling analysis due to geometric limitations (e.g., see Figure 1). The smallest model has 180 atoms and 258 bonds, while the largest model has 3592 atoms and 5312 bonds. Free-free, free-clamped and clamped-clamped boundary conditions are taken into account in vibrational analysis, and axial compression and bending loading conditions are considered in elastic buckling analysis.

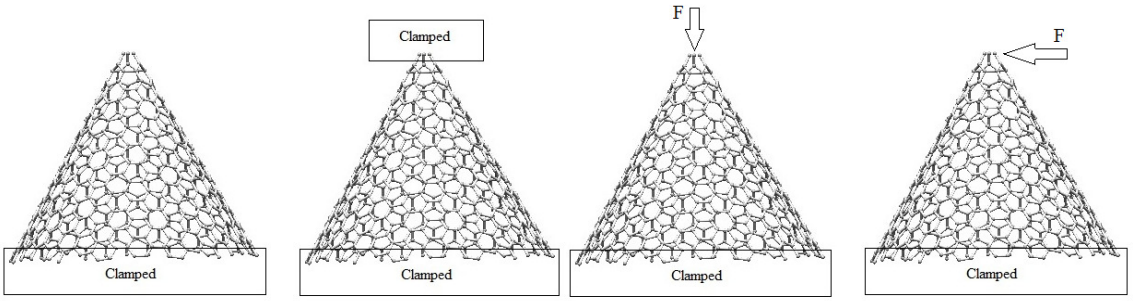

Figure 2: Free-clamped and clamped-clamped boundary conditions in vibrational analysis and axial compression and bending loading conditions in buckling analysis.

Figure 2 shows the boundary and loading conditions for vibrational and buckling analyses of the SWCNCs. All computations of the MM model are completed by using a computer code developed in MATLAB environment, no damping is considered in computational models and the results are verified by using Ansys ® software. After assembling the element stiffness and consistent mass matrices, the natural frequencies and corresponding mode-shapes are obtained by solving the following eigenproblem

$$(\boldsymbol{K}-\omega_i^2\boldsymbol{M})\boldsymbol{d}=\boldsymbol{0} \tag{6}$$

where $\boldsymbol{K}$, $\boldsymbol{M}$, $\boldsymbol{d}$ and ω_i are the global stiffness matrix, global mass matrix, displacement vector and the natural frequencies, respectively. In addition, the natural frequency is equal to $\omega=2\pi f$, where f has the unit of Hertz. Similarly, critical buckling load and corresponding mode shapes are calculated by solving the following eigenproblem

$$(\boldsymbol{K}_0-\lambda\overline{\boldsymbol{K}}_1)\boldsymbol{\psi}=0 \tag{7}$$

where $\boldsymbol{K_0}$ is the global stiffness matrix, $\overline{\boldsymbol{K}}_1$ is the geometric stiffness matrix and $\boldsymbol{\psi}$ is the buckling-mode shape. The factor λ at which buckling occurs is designated as λ_{cr}, and $P_{cr} = \lambda_{cr} P$ [39].

	Present work	Lee and Lee[28]	Mir et al. [29]	Scarpa et al. [34]
Mass matrix type	Consistent	Lumped	Consistent	-
Beam type	Euler-Bernoulli	Shear Beam	Euler-Bernoulli	Shear Beam
Cross-sectional area, A	1.687 Å^2	1.687 Å^2	1.687 Å^2	0.554 Å^2
Density [22]	5.5 x 10^{-27} kg/ Å^3	2.3 x 10^{-27} kg/ Å^3	2.3 x 10^{-27} kg/ Å^3	-
Elastic modulus, E	5.488 x 10^{-8} N/Å^2	5.488 x 10^{-8} N/Å^2	5.488 x 10^{-8} N/Å^2	16.71 x 10^{-8} N/Å^2
Shear modulus, G	8.711 x 10^{-9} N/Å^2	8.711 x 10^{-9} N/Å^2	8.711 x 10^{-9} N/Å^2	80.8 x 10^{-9} N/Å^2
Poisson's ratio, ν	Not needed	0.3	Not needed	0.034
Bond thickness , d	1.47 Å	1.47 Å	1.47 Å	0.84 Å

Table 1: Properties of the beam elements in literature.

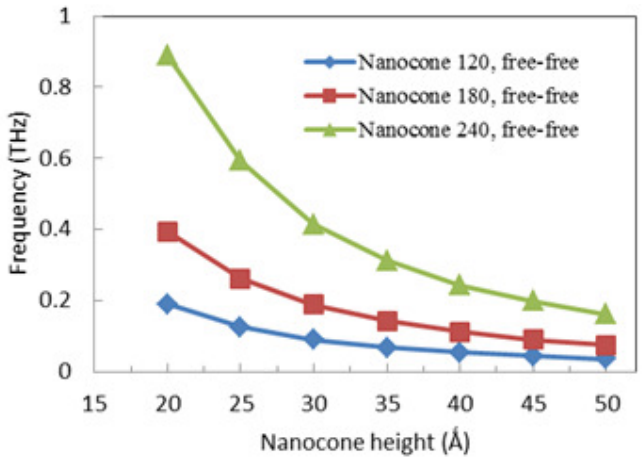

Figure 3: Variation of the first natural frequency of SWCNCs having the disclination angles of 120°, 180° and 240° as the cone height changes for the free-free boundary condition.

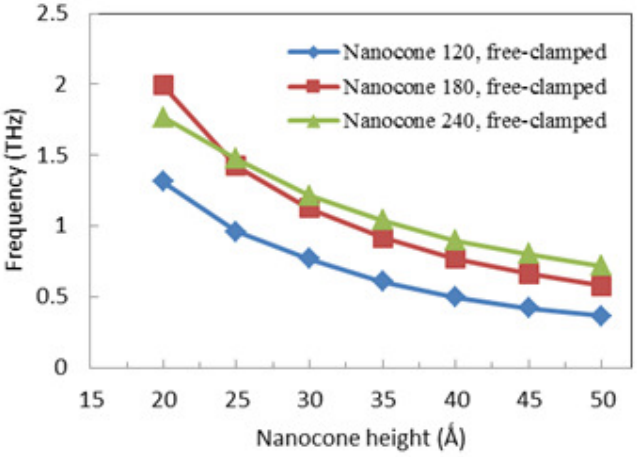

Figure 4: Variation of the first natural frequency of SWCNCs having the disclination angles of 120°, 180° and 240° as the cone height changes for the free-clamped boundary condition.

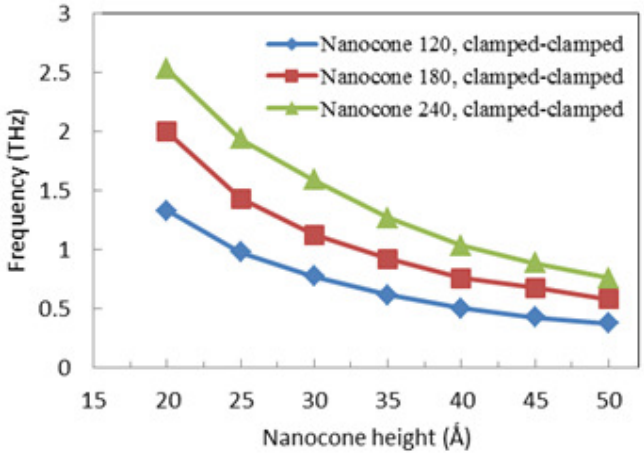

Figure 5: Variation of the first natural frequency of SWCNCs having the disclination angles of 120°, 180° and 240° as the cone height changes for the clamped-clamped boundary condition.

The effects of cone height and disclination angles on the natural frequencies of SWCNCs are examined in vibration analysis where natural frequencies and corresponding mode shapes are obtained. Figures 3, 4 and 5 show the variations of the first fundamental frequencies of SWCNCs versus cone height for free-free, free-clamped and clamped-clamped boundary conditions, respectively. As can be seen in these figures, the first natural frequency decreases with increasing cone height in all types of SWCNCs, whereas it increases as the disclination angle increases except for the SWCNCs having the disclination angle of 240° and height of 20 Å. In addition, the SWCNCs with disclination angles of 240° are more sensitive to variations in height and boundary conditions than the other SWCNCs in vibrational analysis due its small apex angle. When free-clamped and clamped-clamped boundary conditions are considered, the first fundamental frequencies of SWCNCs, are found to be in the range of 0.36 –2.52 THz. Lee and Lee [28] used Timoshenko beam element formulations which include shear deformation effects but they employed Euler-Bernoulli beam element constants (i.e., see Table 1) [23]; this assumption affects the natural frequencies of SWCNC that are found to be lower than those of Euler-Bernoulli beam elements. In addition, density of beam elements is selected to be the density of GSs (i.e. 2300 kg/m3) in the MM model. Hence, natural frequencies of SWCNCs are found to be less than 100GHz in all calculations for the same type of SWCNCs having the height of 20 Å and with free-clamped and clamped-clamped boundary conditions. These frequency ranges are comparable with those of CNTs and SLGSs (i.e., 10 GHz –1.5 THz for SWCNTs and 2.4 GHz – 3.5 THz for SLGSs) which are reported in literature [21, 25].

Figures 6 and 7 show respectively the variations in the first ten natural frequencies for the free-free and clamped-clamped SWCNCs having the height of 50 Å and disclination angles of 120°, 180° and 240°. It is noteworthy that variations in the first ten natural frequencies for the free-clamped SWCNCs which are not presented here for limited space are very close to those of clamped-clamped boundary conditions since relatively small radius of the cone tips has little effect on the vibrational behavior of the SWCNCs for these two boundary conditions.

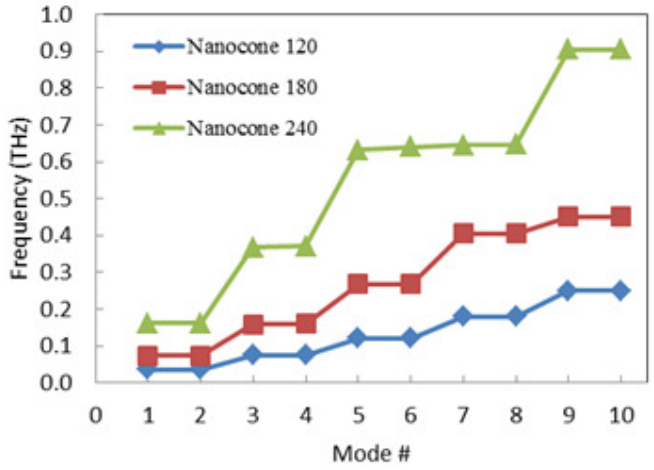

Figure 6: First ten natural frequencies of SWCNCs having the height of 50 Å and disclination angles of 120°, 180° and 240° for free-free boundary condition.

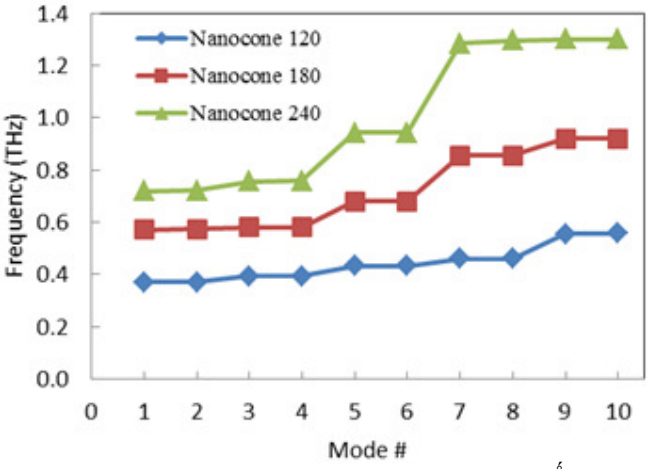

Figure 7: First ten natural frequencies of SWCNCs having the height of 50 Å and disclination angles of 120°, 180° and 240° for clamped-clamped boundary condition.

Figures 8 and 9 show respectively the first five vibration modes of SWCNCs having the disclination angle of 120° and height of 30 Å for the free-free and free-clamped boundary conditions. The mode shapes of clamped-clamped SWCNCs are also similar to those of free-clamped SWCNCs, that are not presented here for limited space. In addition, the second mode shape is very similar to the first mode shape in both figures, that are not presented for limited space as well.

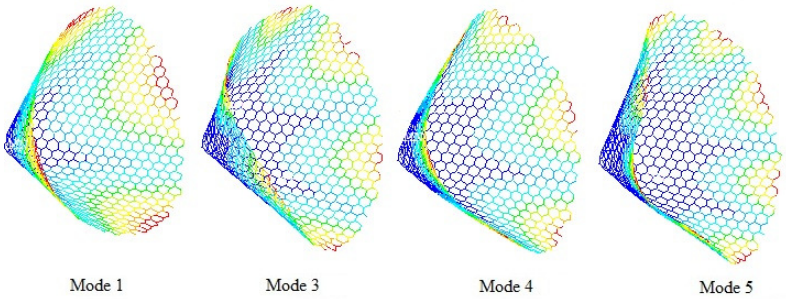

Figure 8: Vibrational modes of SWCNC having the disclination angle of 120°, height of 30 Å for free-free boundary condition.

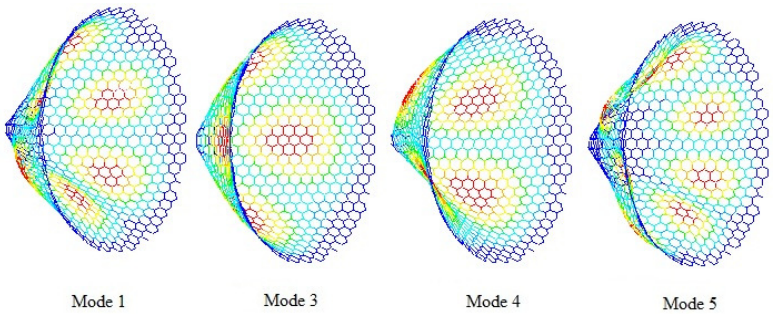

Figure 9: Vibrational modes of SWCNC SWCNC having the disclination angle of 120°, height of 30 Å for free-clamped boundary condition.

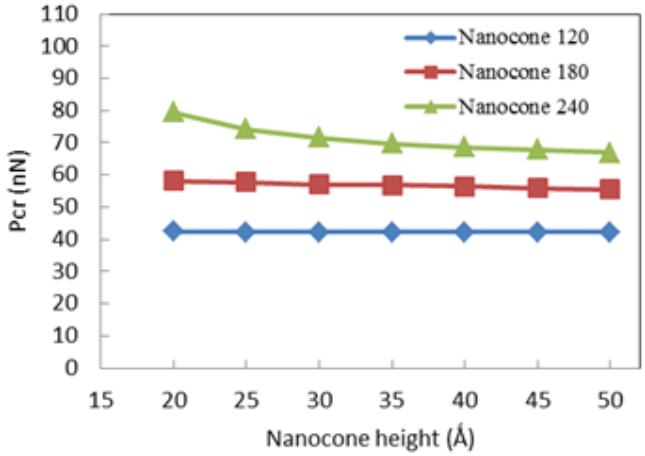

Figure 10: Variation of the first critical buckling load for the SWCNCs having the disclination angles of 120°, 180° and 240° as the cone height changes under axial compression loading condition.

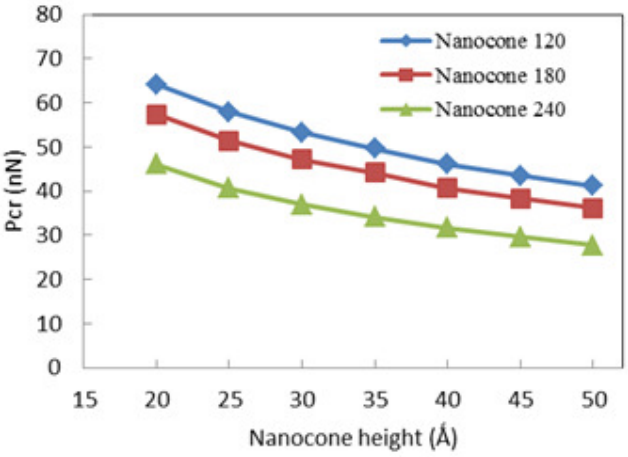

Figure 11: Variation of the first critical buckling load for the SWCNCs having the disclination angles of 120°, 180° and 240° as the cone height changes under bending loading condition.

Similar to vibration analysis, the effects of cone height and disclination angles on the critical buckling load and associated buckling modes of SWCNCs are studied by completing elastic buckling analysis. Figures 10 and 11 show respectively the variations of the first critical

buckling load of SWCNCs as the cone height changes for the axial and bending loading conditions. Buckling analysis results indicate that as the disclination angle increases, the critical buckling load increases in axial compression loading and decreases in bending loading. The buckling load in axial compression is larger than bending load for SWCNCs having the disclination angles of 180° and 240°, and it is smaller than that of bending load for SWCNCs having the disclination angle of 120°. Hence, it is concluded that bending loading is more critical than axial compression loading for buckling behavior of SWCNCs as the disclination angle increases. In addition, the cone height affects the bending buckling forces more than the axial compression buckling forces. The axial and bending buckling forces are found to be in the range of 42 – 79 nN and 27 – 64 nN, respectively. These ranges are comparable with those of CNTs (i.e., ~0.1– 39 nN) which are reported in literature [22].

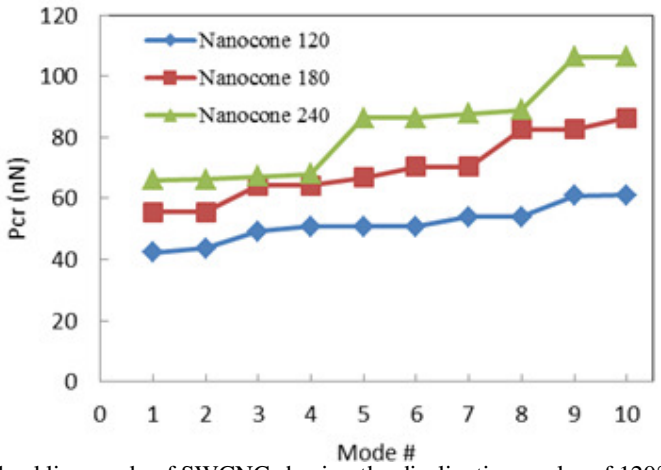

Figure 12: First ten buckling mode of SWCNCs having the disclination angles of 120°, 180° and 240°, and height of 50 Å for the axial loading

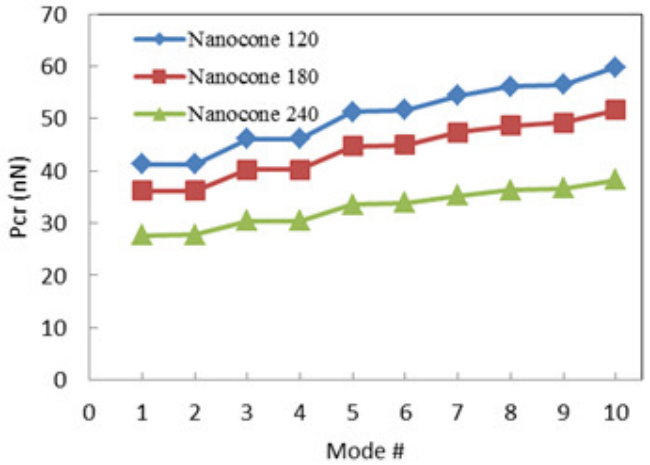

Figure 13: First ten buckling mode of SWCNCs having the disclination angles of 120°, 180° and 240, and height of 50 Å for the bending loading.

Figures 12 and 13 show the first ten buckling loads for the SWCNCs having the height of 50 Å. As can be seen the figures, the elastic buckling modes of the SWCNCs have similar pattern except for the SWCNC with the disclination angle of 240° under axial compression loading.

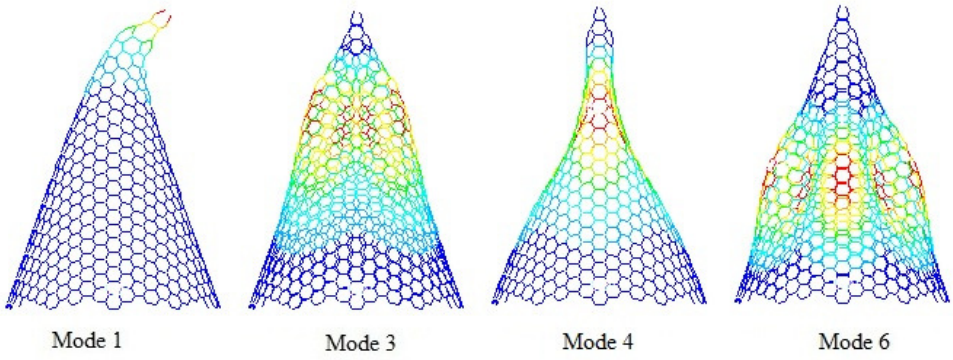

Figure 14: The first six buckling modes of the SWCNC having the disclination angle of 240° under the axial compression loading.

Figures 14 shows the first six buckling modes of the SWCNCs with the disclination angle of 240° and height of 50 Å under the axial compression. Since the second and fifth buckling modes are respectively very similar to the first and sixth buckling modes, they are not presented here for limited space.

3 CONCLUSIONS

In this paper, the elastic buckling and vibration behaviors of SWCNCs are investigated. The MM based FE approach is used to achieve this goal. The axial compression and bending loading conditions are considered in elastic buckling behavior of SWCNCs while free-free, free-clamped and clamped-clamped boundary conditions are considered in vibration analysis of SWCNCs. The effects of cone height and apex angles on the buckling force and natural frequencies of SWCNCs are also studied. Vibration analysis results indicate that the natural frequency decreases with increasing cone height in all types of SWCNCs, whereas it increases as the disclination angle increases. Buckling analysis results indicate that as the disclination angle increases, the critical buckling load increases in axial compression loading and decreases in bending loading. In addition, it is observed that bending loading is more critical than axial compression loading for buckling behavior of SWCNCs if the disclination angle increases. When free-clamped and clamped-clamped boundary conditions are considered, fundamental frequencies of the SWCNCs are found to be in the range of 0.36 –2.52 THz. The axial and bending buckling forces are found to be in the range of 42 – 79 nN and 27 – 64 nN, respectively. These results are comparable with the results for CNTs and SLGSs in literature in most cases and it can be used in designing atomic force microscope (AFM) and scanning tunneling microscope (STM) tips. In the future, fracture and transient dynamics analyses can be performed in order to evaluate the damage and dynamic behavior of SWCNCs. Moreover, Morse potential can be employed in the MM model for large deformation problems.

REFERENCES

[1] S. Iijima, Helical microtubules of graphitic carbon. *Nature*, **354**, 56-58, 1991.

[2] S.P. Jordan, V.H. Crespi, Theory of carbon nanocones: mechanical chiral inversion of a micron-scale three-dimensional object. *Physical Review Letters*, **93,** 255504, 2004.

[3] P.E. Lammert, V.H. Crespi, Graphene cones: Classification by fictitious flux and electronic properties. *Physical Review B,* **69**, 035406, 2004.

[4] S. Berber, Y.K. Kwon, D. Tomanek, Electronic and structural properties of carbon nanocones. *Physical Review B,* **62**, 2291-2294, 2000.

[5] N. Yang, G. Zhang, B. Li, Carbon nanocone: A promising thermal rectifier. *Applied Physics Letters,* **93,** 243111, 2008.

[6] D. Kumar, V. Verma, H.S. Bhatti, K., 2011 Elastic moduli of carbon nanohorns. *Journal of Nanomaterials*, **2011**, 127952, 2011.

[7] J.X. Wei, K.M. Liew, X.Q. He, Mechanical properties of carbon nanocones. *Applied Physics Letters*, **91**, 261906, 2007.

[8] M. Ge, K. Sattler, Observation of fullerene cones. *Chemical Physics Letters,* **220**, 192-196, 1994.

[9] A. Krishnan, E. Dujardin, M.M.J. Treacy, J. Hugdahl, S. Lynum, T. W. Ebbesen, Graphitic cones and the nucleation of curved carbon surface. *Nature*, **388**, 451-454, 1997.

[10] J. Sripirom, S. Noor, U. Köhler, A. Schulte, Easy made and handled carbon nanocones for scanning tunneling microscopy and electroanalysis. *Carbon,* **49,** 2402-2412, 2011.

[11] C. Chen, L.H. Chen, X.R. Ye, C. Daraio, S. Jin, C.A. Orme, A. Quist, R. Lal, Extreme sharp carbon nanocone probe for atomic force microscopy imaging. *Applied Physics Letters,* **88**, 153102, 2006.

[12] J.Y. Hsieh, C. Chen, J.L. Chen, C.I. Chen, C.C. Hwang, The nanoindentation of a copper substrate by single-walled carbon nanocone tips: A molecular dynamics study. *Nanotechnology,* **20** 095709, 2009.

[13] S.S. Yu, W. T. Zheng, Effect of N/B doping on the electronic and field emission properties for carbon nanotubes, carbon nanocones, and graphene nanoribbons. *Nanoscale*, **2** 1069, 2010.

[14] P.C. Tsai, T.H. Fang, A molecular dynamics study of the nucleation, thermal stability and nanomechanics of carbon nanocones. *Nanotechnology,* **18**, 105702, 2007.

[15] K.M. Liew, J.X. Wei, X.Q. He, Carbon nanocones under compression: Buckling and post-buckling behaviors. *Physical Review B,* **75**, 195435, 2007.

[16] M.L. Liao, C.H. Cheng, Y.P. Lin, Tensile and compressive behaviors of open-tip carbon nanocones under axial strains. *Journal of Materials Research,* **26**, 1577-1584, 2011.

[17] R.D.F. Abadi, M.M. Fotouhi, H. Haddadpour, Free vibration analysis of nanocones using nonlocal continuum model. *Physics Letters A,* **375,** 3593-3598, 2011.

[18] G.M. Odegard, T.S. Gates, L.M. Nicholson, K.E. Wise, Equivalent-continuum modeling of nano-structured materials. *Composite Science and Technology,* **62**, 1869–1880, 2002.

[19] C. Li, T.W. Chou, A structural mechanics approach for the analysis of carbon nanotubes International. *Journal Solids Structures*, **40**, 2487–2499, 2003.

[20] C. Li, T.W. Chou, Vibrational behaviors of multiwalled-carbon-nanotube-based nanomechanical resonators. *Applied Physics Letters,* **84**, 12, 2004.

[21] C. Li, T.W. Chou, Single-walled carbon nanotubes as ultrahigh frequency nanomechanical resonators. *Physical Review B*, **68**, 073405, 2003.

[22] C. Li, T.W. Chou, Modeling of elastic buckling of carbon nanotubes by molecular structural mechanics approach. *Mechanics of Materials*, **36**, 1047-1055, 2004.

[23] K.I. Tserpes, P. Papanikos, Finite element modeling of single-walled carbon nanotubes. *Composites Part B*, **36**, 468–477, 2005.

[24] K. Hashemnia, M. Farid, R. Vatankhah, Vibrational analysis of carbon nanotubes and single-layered graphene sheets using molecular structural mechanics approach. *Computational Materials Science*, **47**, 79-85, 2009.

[25] A. Sakhaee-Pour, M.T. Ahmadian, R. Naghdabadi, Vibrational analysis of single-layered graphene sheets. *Nanotechnology*, **19**, 085702, 2008.

[26] A. Sakhaee-Pour, M.T. Ahmadian, A. Vafai, Vibrational analysis of single-walled carbon nanotubes using beam element. *Thin-Walled Structures*, **47**, 646-652, 2009.

[27] A. Sakhaee-Pour, Elastic buckling of single-layered graphene sheet. *Computational Material Science*, **45**, 266-270, 2009.

[28] J.H. Lee, B.S. Lee, Modal analysis of carbon nanotubes and nanocones using FEM. *Computational Materials Sciences*, **51**, 30-42, 2012.

[29] M. Mir, A. Hosseini, G. Majzoobi, A numerical study of vibrational properties of single-walled carbon nanotubes. *Computational Materials Science,* **43**, 540-548, 2008.

[30] H.C. Cheng, Y.L. Liu, Y.C. Hsu, W.H. Chen, Atomistic-continuum modeling for mechanical properties of single-walled carbon nanotubes. *International Journal of Solids and Structures*, **46**, 1695-1704, 2009.

[31] C.W. Fan, Y.Y. Liu, C. Hwu, Finite element simulation for estimating the mechanical properties of multi-walled carbon nanotubes. *Applied Physics A*, **95**, 819-831, 2009.

[32] A.F. Avila, A.C. Eduardo, A.S. Neto, Vibrational analysis of graphene based nanostructures. *Computer and Structures,* **89**, 878-892, 2011.

[33] C. Baykasoglu, A. Mugan, Dynamic analysis of single-layer graphene sheets. *Computational Material Science,* **55**, 228-236, 2012.

[34] F. Scarpa, S. Adhikari, A mechanical equivalence for Poisson's ratio and thickness of C-C bonds in single wall carbon nanotubes. *Journal of Physics D: Applied Physics,* **41,** 085306, 2008.

[35] F. Scarpa, S. Adhikari, A.S. Phani, Effective elastic mechanical properties of single layer graphene sheets. *Nanotechnology*, **20**, 065709, 2009.

[36] G. Brinkmann, N.V. Cleemput, Classification and generation of nanocones. *Discrete Applied Mathematics*, **159**, 1528-1539, 2011.

[37] B. Ekşioğlu, A. Nadarajah, Structural analysis of conical carbon nanofibers. *Carbon*, **44,** 360-373, 2006.

[38] P.J.F. Harris, *Carbon nanotubes and related structures*. Cambridge University Press Cambridge UK, 1999.

[39] T.J.R. Hughes, *The finite element method, linear static and dynamic finite element analysis*. Prentice-Hall, 2000.